Supporting Information

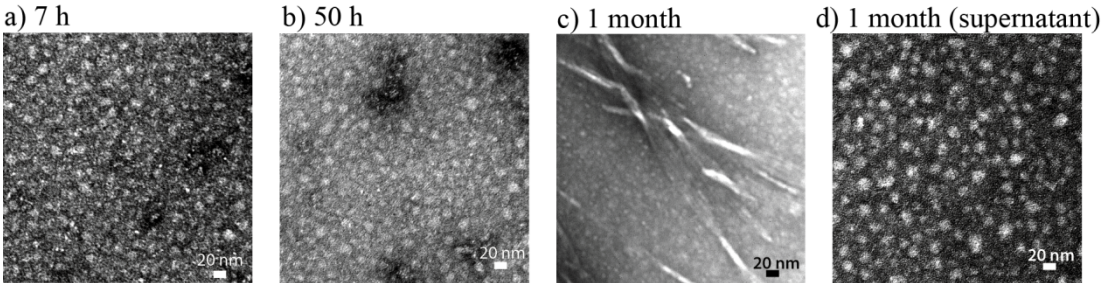

Figure S1. TEM images of 32 μM Aβ42 in 10 mM phosphate buffer (pH 7.5, 0.02% w/v NaN_3) at 4 °C at incubation times of (a) 7 h, (b) 50 h and (c, d) 1 month. The sample was ^{13}C- and ^{15}N-uniformly-labeled at Phe20, Ala21, Val24, Gly25, and Leu34, for SSNMR sample preparation (Fig. 2c). The results show that no fibril species were formed before 50 h of incubation, which is consistent with ThT fluorescence results in Fig. 1.

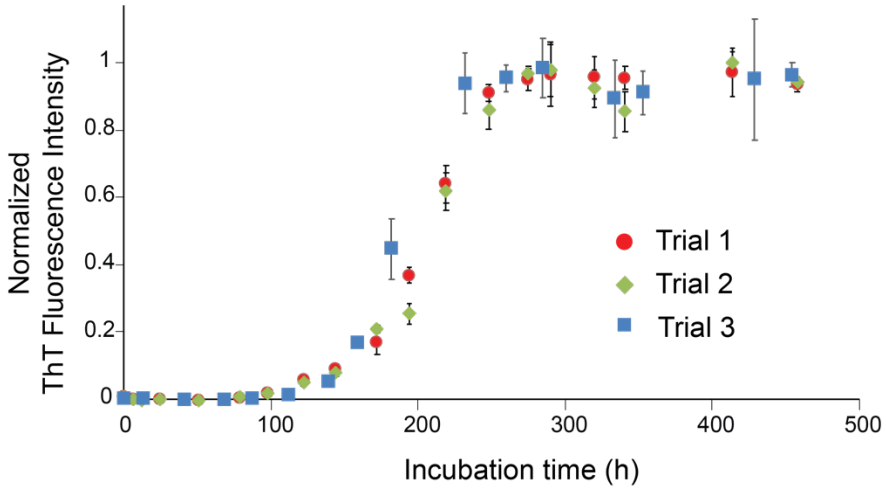

Figure S2. Incubation-time dependence of ThT fluorescence for Aβ42 in 10 mM phosphate buffer (pH 7.5, 0.02% w/v NaN_3) at 4 °C. The three trials were performed for 29 μM Aβ42 (Trials 1–2) and 51 μM Aβ42 (Trial 3). The data for Trial 1 are the same as those for Fig. 1a.

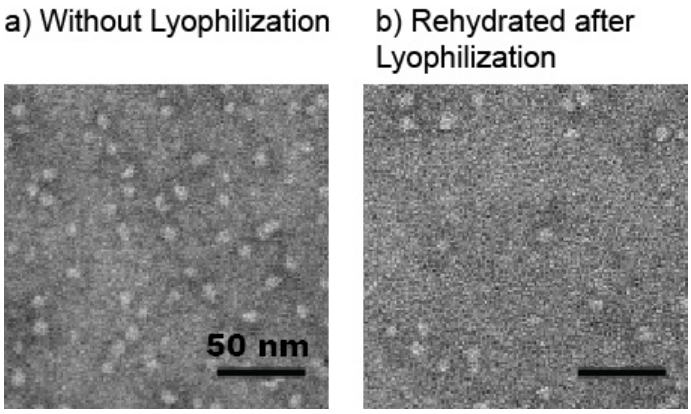

Figure S3. TEM images of SPA samples obtained (a) without lyophilization (i.e. hydrated) and (b) with rehydration after lyophilization. Nearly identical images were obtained. A 5.0-μL aliquot of sample was mixed with 5.0 μL of Nano-W negative stain (Nanoprobes, NY) on a sputter coated formvar coated 200-mesh copper grid stabilized with carbon film (EMJapan) for 2 min. Excess solutions were removed with a filter paper and air dried for 1 min. Samples were analyzed using a JEOL JEM-1400Plus electron microscope at an accelerating voltage of 80 kV and a magnification of 100,000× at the Biomaterials Analysis Division of Tokyo Institute of Technology.

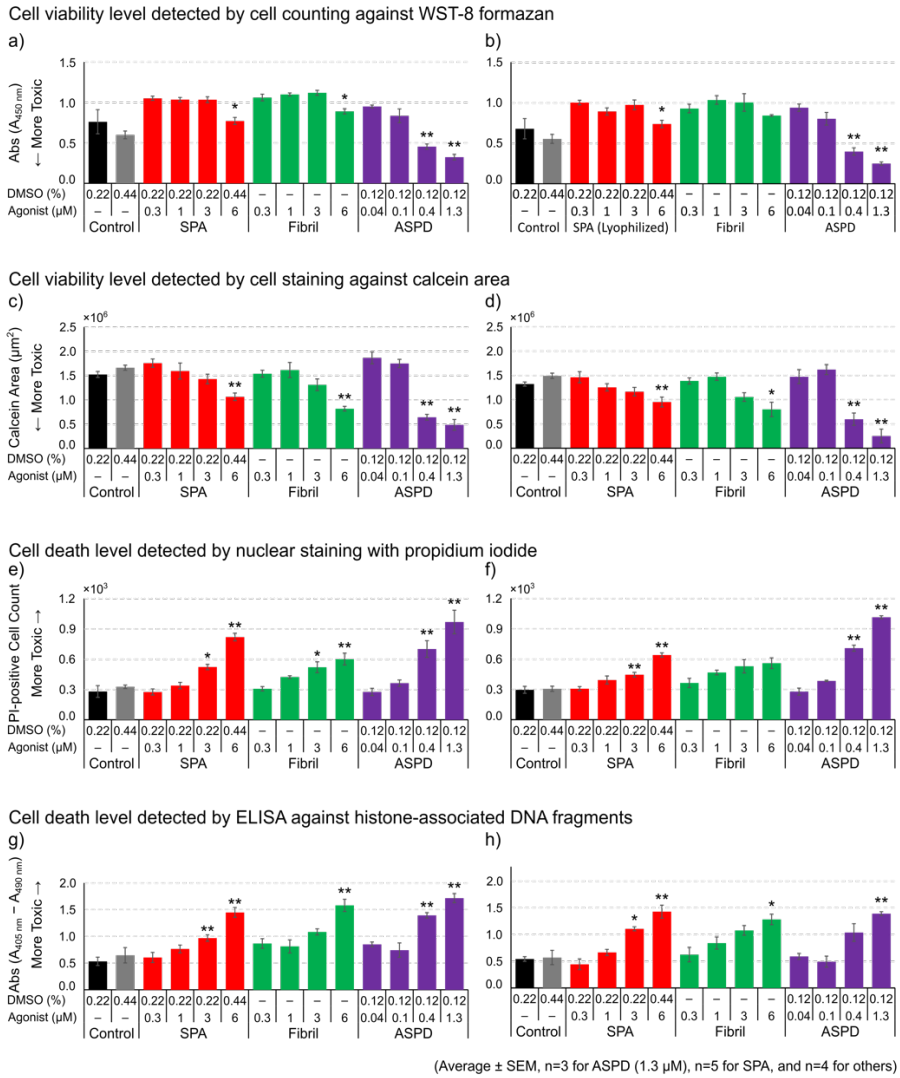

Figure S4. Cell viability levels were detected (a, b) by cell counting against WST-8 formazan and (c, d) by cell staining against calcein area on primary culture of rat hippocampal neural cells for SPA (red) compared with that for fibril (green), and ASPD (purple) at varied agonist concentrations (calculated in terms of Aβ monomer mass 4.5 kDa). Cell death levels were detected (e, f) by nuclear staining with propidium iodide and (g, h) by ELISA against histone-associated DNA fragments on cultured rat hippocampal cells for SPA (red) compared with that for fibril (green), and ASPD (purple) at varied agonist concentrations. SPA without lyophilization was used for (a, c, e, g). SPA with lyophilization was used for (b, d, f, h). Statistical analyses were performed using Sceffe's F test. Single (*) and double (**) asterisks denote the *p*-value of less than 0.05 and 0.01 ($p < 0.05$ and $p < 0.01$, Scheffe's F test), respectively. SPA samples at 6 μM were compared with the control with 0.44% DMSO, and other SPA samples were compared with that with 0.22% DMSO due to relatively high concentration of DMSO used in the incubation. Fibril and ASPD samples were compared with their respective samples at the lowest concentrations (i.e. 0.3 μM for fibril and 0.04 μM for ASPD) as controls in order to determine the concentration-dependent toxicity based on an assumption that the toxicity is negligible at their lowest concentrations.

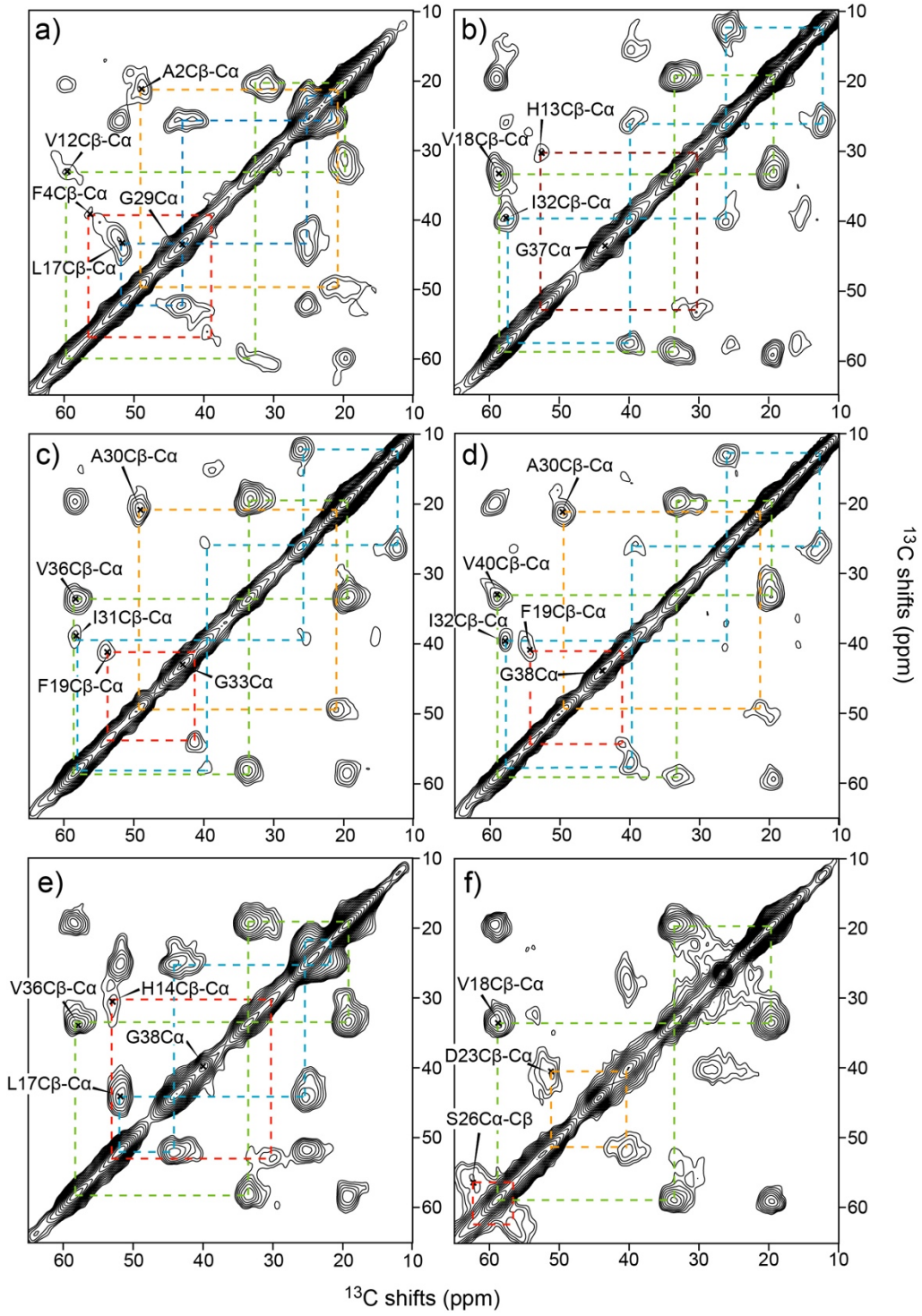

Figure S5. Two-dimensional (2D) SSNMR analysis of Aβ42 SPA samples in different ^{13}C- and ^{15}N-isotope labeling schemes. The sample was obtained 12 h after incubation of Aβ42 with phosphate buffer at 4 °C. (a–f) 2D ^{13}C-^{13}C correlation SSNMR spectra of SPA samples that were uniformly labeled with ^{13}C and ^{15}N at (a) Phe4, Val12, Leu17, Ala21 and Gly29, (b) His13, Val18, Ile32 and Gly37, (c) Phe19, Ala30, Ile31, Gly33 and Val36, (d) Phe19, Ala30, Ile32, Gly38 and Val40, (e) His14, Leu17, Val36 and Gly38, and (f) Val18, Asp23, Ser26 and Lys28. All data were apodized with a Lorenz-to-Gauss window function with an inverse exponential line-narrowing function of 30 Hz and a Gaussian broadening function of 120 Hz in both the t_2 and t_1 domains. The overall experimental time was 24–72 h.

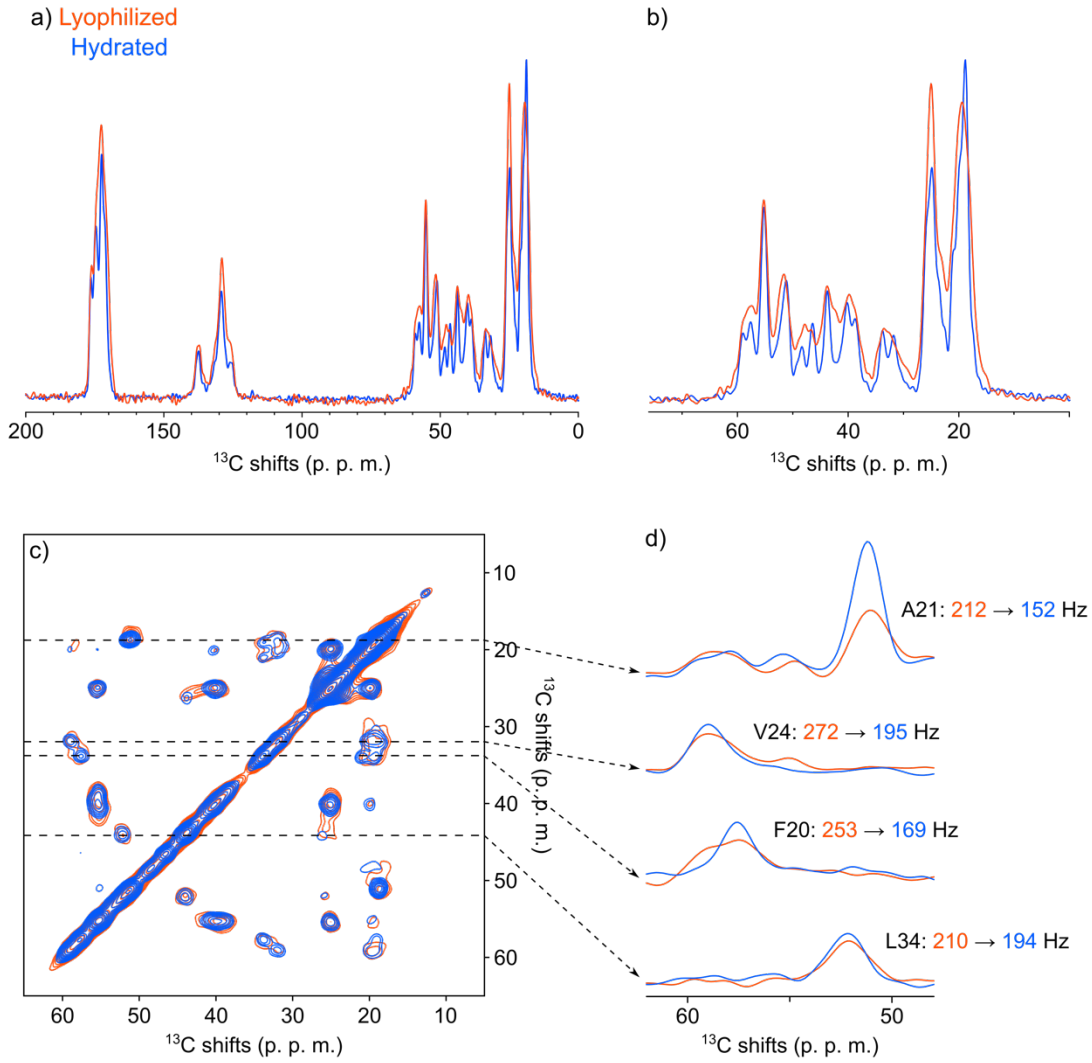

Figure S6. (a) 1D ^{13}C CP MAS spectra of lyophilized (red) and hydrated (blue) Aβ42 fibril that was uniformly labeled with ^{13}C and ^{15}N at Phe20, Ala21, Val24, Gly25, and Leu34. (b) Extraction of the aliphatic region from (a). The fibril sample was prepared by incubation at a room temperature in order to examine the effect of hydration. (c) 2D ^{13}C SSNMR chemical shift correlation spectra of the lyophilized (red) and hydrated (blue) Aβ42 fibril with the same isotopic labeling scheme. (d) 1D slices from (b) selected at the C_β chemical shift of Ala21, Val24, Phe20, and Leu34 (dotted lines). Line widths of the cross peaks were shown for lyophilized (red) and hydrated (blue) samples. All data were apodized with a Lorentz-to-Gauss window function with an inverse exponential line-narrowing function of 30 Hz and a Gaussian broadening function of 120 Hz in both the t_2 and t_1 domains.

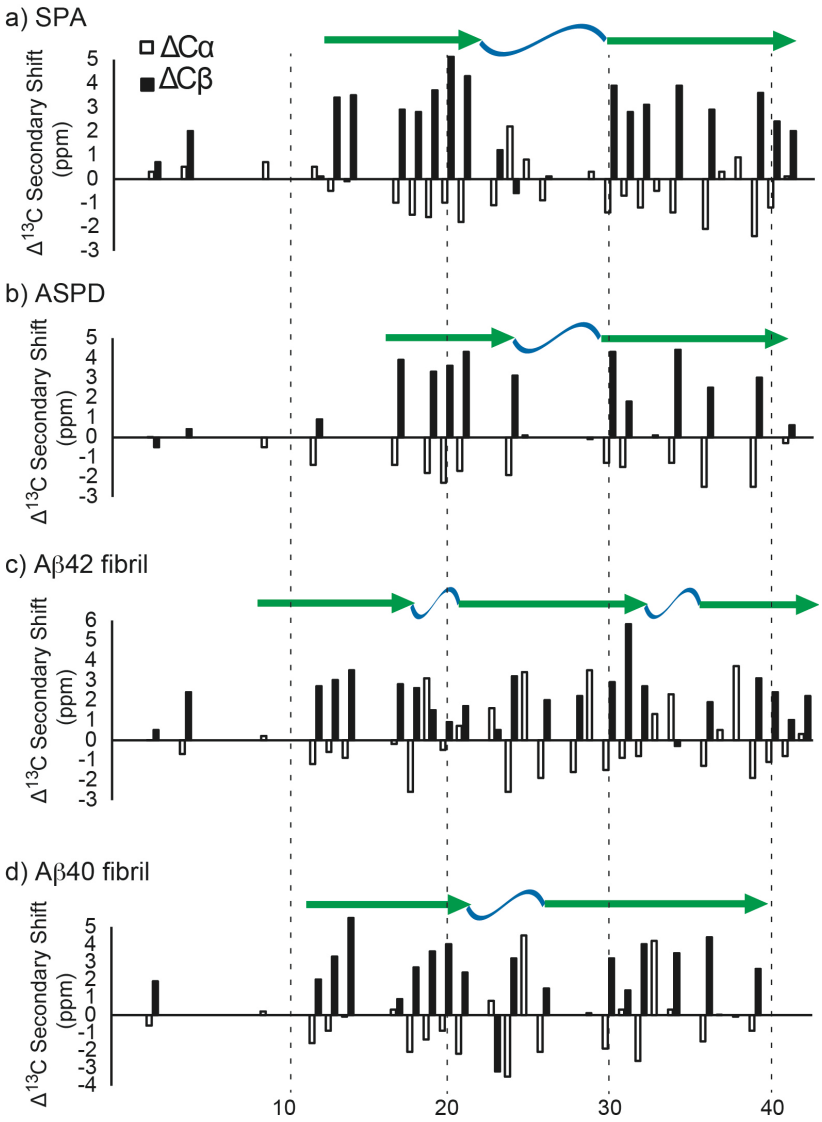

Figure S7. (a–d) Secondary ^{13}C chemical shifts for $^{13}C_{\alpha}$ (black bars) and $^{13}C_{\beta}$ (white bars), observed by SSNMR for the Aβ42 in (a) SPA, (b) ASPD, (c) RT fibril, and d) Aβ40 in fibrils with the corresponding secondary structures based on TALOS-N analysis.[1]

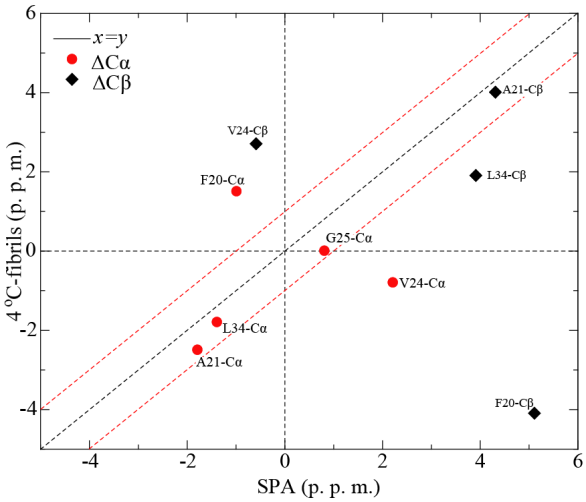

Figure S8. A comparison of ^{13}C secondary shifts between SPA and LT-fibril samples. The secondary $^{13}C_{\alpha}$ (red), $^{13}C_{\beta}$ (black) chemical shifts of LT-fibril were plotted against that of SPA along with $y = x$ (black dashed line) and $y = x \pm 1$ (red dashed lines). The ΔC_{β} shifts of Leu34, and both ΔC_{α} and ΔC_{β} shifts of Phe20 and Val24 were found to be quite different of SPA from LT-fibril, indicating conformational diversity.

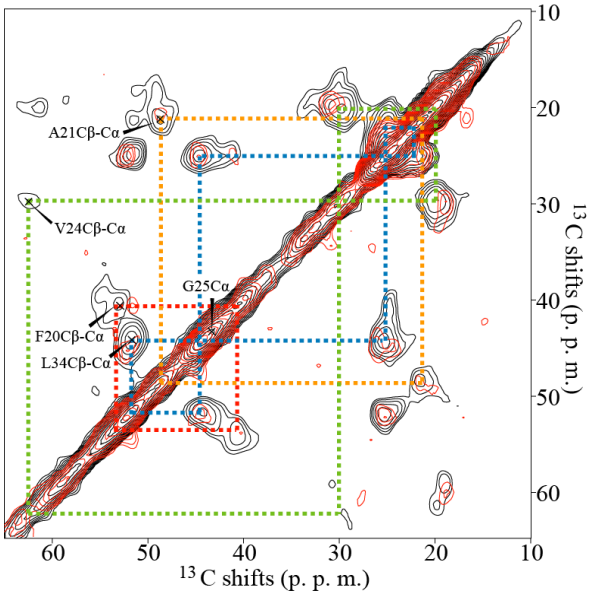

Figure S9. A comparison of 2D ^{13}C-^{13}C correlation SSNMR spectra of SPA harvested at ~12 h (black spectrum) and lyophilized supernatant sample collected after 1-month incubation (red spectrum). The data were apodized with a Lorenz-to-Gauss window function with an inverse exponential line-narrowing function of 30 Hz and a Gaussian broadening function of 120 Hz in both the t_2 and t_1 domains. The overall experimental time was 72 h. Both samples were uniformly labeled with ^{13}C and ^{15}N at (a) Phe20, Ala21 Val24, Gly25, and Leu34.

Supplemental tables

Table S1. Summary of SSNMR sample and spectrum information of SPA and fibril samples of Aβ42.

Labeling Scheme	Samples[a)]	Number of scans per t_1 point	Dry sample amount (mg)[a)]	Baseline level with respect to the noise level[b)]
A2G9F20V39I41	SPA	400	19.0	5.2
F4V12L17**A21**G29	SPA	552	13.6	3.2
H13V18I32G37	SPA	416	15.2	4.5
H14L17I23G38	SPA	624	29.0	5
V18D23S26K28	SPA	1728	14.1	4
F19A30I31G33V36	SPA	608	17.8	5
F19A30I32G38V40	SPA	472	19.5	4
F20**A21**V24G25L34	SPA	528	14.4	4
F20**A21**V24G25L34	4 °C-fibrils	96	7.5	6
F20**A21**V24G25L34	1-m SPA	632	23.7	3
F20**A21**V24G25L34	triple-β fibrils	184	7.6	7

a) The actual dry sample packed into an SSNMR rotor. The weight includes both protein sample and salts from the solvent.

b) Baseline level is normally set from 4–8 times higher than the noise level to ensure all the signals are observable and all the noises are excluded. For 50 ms mixing DARR spectrum, the baseline level of SPA sample with labeling scheme of F4V12L17A21G29 is lowered to enable the observation of the weak aliphatic cross peaks of Phe4.

Table S2. ^{13}C chemical shifts and predicted torsion angles of Aβ42 in SPA.

Residue	Chemical shifts (ppm) [a]									Torsion angles (degree) [b]	
	CO	C_α	C_β	C_γ	C_δ	C_ε	C_ζ	$C_{\gamma 2}$	$C_{\delta 2}$	Φ	ψ
A2	173.9	50.8	17.8								
F4	NA	56.2	39.6	137.5	129.2	129.2	123.4				
G9	171.1	43.8									
V12	173.9	60.7	31.0	19.9				19.9		-77.4±21.6*	140.4±12.5*
H13	171.6	52.5	30.4	136.1	115.0	129.5				-112.6±19.0*	142.7±15.0*
H14	172.7	52.9	30.8	134.6		126.4				-106.2±23.5*	145.3±13.6*
L17	171.2	52.1	43.3	25.2					21.9	-122.2±14.3	135.9±10.5
V18	172.1	58.7	33.7	19.3				19.3		-121.5±11.3	136.2±13.0
F19	171.4	54.1	41.3	137.4	130.7	128.3	116.6			-120.0±12.1	145.0±12.3
F20	171.5	54.7	42.7	137.2	129.2	129.2	125.5[c]			-131.4±9.7	151.8±8.9
A21	173.2	48.7	21.4							-140.5±12.4	154.8±11.3
E22										-72.4±12.9	140.3±10.1
D23	174.5	51.1	40.3	177.9						-87.7±26.5*	157.7±20.9*
V24	174.0	62.4	30.3	19.8						-58.3±7.2	132.5±5.0
G25	171.0*	43.9								79.6±48.4*	-23.1±42.9*
S26	172.6	55.4	61.9							-70.9±13.4*	140.6±13.3*
G29	171.2	43.4								86.8±6.2*	3.5±9.1
A30	173.1	49.1	21.0							-115.4±15.4	147.0±14.5
I31	172.5	58.4	39.6	25.3	12.5			15.4		-122.5±15.6	134.6±11.8
I32	172.2	57.9	39.9	26.1	12.3			15.6		-127.6±11.8	141.7±12.4
G33	169.1	42.6								-128.0±33.1	159.0±15.4
L34	172.4	51.7	44.3	25.3					21.9	-127.5±8.9	137.9±13.0
M35										-98.1±12.9	126.1±11.4
V36	172.3	58.1	33.8	19.4				19.4		-126.5±11.8	141.0±12.0
G37	169.5	43.4								-155.1±21.5	170.6±14.0
G38	169.3	44.0								-165.7±27.9	175.1±17.6
V39	172.0	57.8	34.5	19.8				19.8		-135.7±10.2	145.2±12.6
V40	172.4	59.0	33.3	19.7				19.7		-118.0±13.6	132.8±8.2
I41	172.2	59.2	38.8	26.3	12.3			16.4		-108.4±15.7	134.6±10.7

a) ^{13}C chemical shifts were referenced to neat TMS reference, which is off from the DSS reference by 2.01 ppm.[2-3] ^{15}N shifts were referenced to liquid NH_3.[3]

b) Elucidated from TALOS-N analysis. The angles marked by * were predicted with "Warning" or as "Dynamic" regions.

c) Partially overlapping with the shoulder of F20C_ε and C_δ peaks.

d) Errors of the chemical shifts were estimated to be ±0.01 ppm.

References:

1. Shen, Y.; Bax, A., Protein backbone and sidechain torsion angles predicted from NMR chemical shifts using artificial neural networks. *J Biomol NMR* **2013,** *56* (3), 227-241.
2. Morcombe, C. R.; Zilm, K. W., Chemical shift referencing in MAS solid state NMR. *J. Magn. Reson.* **2003,** *162* (2), 479-486.
3. Harris, R. K.; Becker, E. D.; De Menezes, S. M. C.; Granger, P.; Hoffman, R. E.; Zilm, K. W., Further conventions for NMR shielding and chemical shifts IUPAC recommendations 2008. *Solid-state NMR* **2008,** *33* (3), 41-56.